Using Airborne Laser Scanner and Path Length Distribution Model to Quantify Clumping Effect and Estimate Leaf Area Index

Ronghai Hu, Guangjian Yan, *Senior Member, IEEE*, Françoise Nerry, Yunshu Liu, Yumeng Jiang, Shuren Wang, Yiming Chen, Xihan Mu, Wuming Zhang, and Donghui Xie

***Abstract*— The airborne laser scanner (ALS) provides great potential for mapping the leaf area index (LAI) at the landscape scale using grid cell statistics, while its application is restricted by the lack of clumping information, which has been an unsolved issue highlighted for a long time. ALS generally provides an effective LAI because its footprint is too large to capture small gaps to apply traditional ground-based clumping correction methods. Here, we present a grid cell method based on path length distribution model to calculate the clumping-corrected LAI using ALS data without the requirement of additional field measurements. We separated the within- and between-crown areas to consider between-crown clumping, and used the path length distribution as estimated by local canopy height distribution to consider 3-D foliage profile and within-crown clumping. The path length distribution model takes advantage of the 3-D information rather than the gap size distribution, thus avoiding the limitation of large ALS footprint. With the 0.4-m-footprint ALS data, the results are generally promising and a multilevel clumping analysis is consistent with landscape flown. The ALS LAIs of different resolutions are consistent, with a difference of less than 5% from 5- to 250-m resolutions. Due to its consistency and simple configuration, the method provides an opportunity to map the clumping-corrected LAI operationally and strengthens the ability of airborne lidar to monitor vegetation change and validate the satellite product. This grid cell method based on path length distribution is worth further testing and application using more recent laser technology.**

***Index Terms*— Airborne laser scanner (ALS), clumping, leaf area index (LAI), lidar, path length distribution.**

Manuscript received October 15, 2017; revised January 7, 2018; accepted January 12, 2018. Date of publication March 26, 2018; date of current version May 21, 2018. This work was supported in part by the Key Program of the National Natural Science Foundation of China (NSFC) under Grant 41331171, in part by the National Basic Research Program of China under Grant 2013CB733402, in part by the NSFC under Grant 61227806 and Grant 41401410, and in part by the China Scholarship Council. *(Corresponding author: Guangjian Yan.)*

R. Hu is with the State Key Laboratory of Remote Sensing Science, jointly sponsored by Beijing Normal University and Institute of Remote Sensing and Digital Earth of Chinese Academy of Sciences, Beijing 100875, China, with the Beijing Engineering Research Center for Global Land Remote Sensing Products, Institute of Remote Sensing Science and Engineering, Faculty of Geographical Science, Beijing Normal University, Beijing 100875, China, and also with the ICube Laboratory, UMR 7357 CNRS-University of Strasbourg, F-67412 Illkirch, France (e-mail: sea@mail.bnu.edu.cn).

G. Yan, Y. Liu, Y. Jiang, S. Wang, Y. Chen, X. Mu, W. Zhang, and D. Xie are with the State Key Laboratory of Remote Sensing Science, jointly sponsored by Beijing Normal University and Institute of Remote Sensing and Digital Earth of Chinese Academy of Sciences, Beijing 100875, China, and also with the Beijing Engineering Research Center for Global Land Remote Sensing Products, Institute of Remote Sensing Science and Engineering, Faculty of Geographical Science, Beijing Normal University, Beijing 100875, China (e-mail: gjyan@bnu.edu.cn).

F. Nerry is with the ICube Laboratory, UMR 7357 CNRS-University of Strasbourg, F-67412 Illkirch, France (e-mail: f.nerry@unistra.fr).

Color versions of one or more of the figures in this paper are available online at http://ieeexplore.ieee.org.

Digital Object Identifier 10.1109/TGRS.2018.2794504

I. Introduction

LEAF area index (LAI), defined as one half of the total leaf area per unit ground surface area, is a key vegetation parameter for modeling mass (water and carbon) and energy (radiation and heat) exchange between the biosphere and the atmosphere [1]–[6].

LAI estimation has been achieved from ground to satellite levels, while its accurate estimation is still difficult at landscape or regional scales. Indirect ground-level methods based on Beer's law, which utilizes the gap probability measured by optical instruments, are convenient and fast for measuring the LAI at scales from tens to hundreds of meters [7]–[11]. However, they are impractical for measuring the LAI over larger scales due to time, cost, and labor limitations. Spaceborne or airborne passive optical remote sensing, which is based on physical vegetation models or empirical relationships between vegetation indices, is able to map the LAI over larger scales [12]–[15]. Passive optical remote sensing is valuable for global and regional studies, but its accuracy and consistency are limited by several other factors, such as atmosphere, soil, and underlying vegetation; thus, calibration and validation are always required [16]–[19]. Indirect ground measurement provides an alternative, but it cannot provide spatially continuous validation data.

The airborne laser scanner (ALS), also commonly known as airborne lidar, provides a great opportunity to accurately map the LAI due to its ability to penetrate canopies and its fast coverage over large areas [20]. Its penetrating ability allows it to better characterize the interior canopy, thus alleviating the saturation problem [21]–[23]. The similarity between lidar penetration rate and gap fraction also provides an opportunity to use the well-developed methods in indirect LAI measurements that are based on Beer's law. In the past decade, gap fraction-based methods have been introduced in lidar measurements to derive the LAI and found to be superior to allometric or empirical methods [24]–[29].

While much progress has recently been achieved, the vast majority of airborne lidar work estimates effective LAI (LAIe) rather than the actual LAI. Correcting clumping effect is still an unsolved and highlighted issue in airborne lidar studies. The LAIe is calculated as a negative logarithm of gap probability or transmittance, which is originally used to model the LAI inhomogeneous scene based on Beer's law. The clumping effect of leaves, however, will increase the gap probability, and thus, the LAIe will be smaller than the actual LAI. Under these circumstances, the LAIe is the LAI of a hypothetical homogeneous canopy with an identical gap probability of the clumped canopy. And the clumping index is defined as the quotient of the LAIe to the actual LAI [30], [31]. For LAI mapping, 3-D discrete airborne lidar data were generally gridded into an image with a grid size of tens of meters [28], [32], which generally covers several tree crowns and large gaps between crowns. Thus, both between-crown and within-crown clumping exist in each grid cell. The need for modeling and quantifying the clumping effect has been highlighted for airborne lidar research for a long time [22], [32]–[36]. To make comparisons with the true LAI, empirical values [37], [38] and ground measurements [39] have been adopted. However, the clumping index is a variable parameter that changes with observation direction, location, scale, and season, even in the same forest [8], [31], [40], [41]. Very few attempts have been made to quantify the clumping effect using airborne lidar, those that have included performing regression analyses with vegetation indices [42] and implementing the traditional ground method with gap size information [43]. The correlations between airborne and ground measurements were found to be good. However, the lidar-based clumping index is still different from the ground clumping index and thus, field measurements are still needed for regression in these methods [42], [43]. In addition, the results of airborne lidar are generally worse due to the low point density [43]. Although much progress has been achieved, these methods did not quantify the clumping effect using airborne lidar independently, which restricts airborne lidar from operationally monitoring vegetation.

The large footprint and low point density of airborne lidar are two major constraints for applying the traditional ground method to correct the clumping effect, as airborne lidar footprints (tens of centimeters or larger) are too large to capture the small gaps [28] and the detailed gap size distribution, even if it is possible to resolve the average gap probability. In addition, the 3-D information is also not utilized efficiently. The 3-D information is often converted to a 2-D binary image to use the traditional gap distribution-based method [43].

The recently developed path length distribution model [7] provides a potential solution for correcting clumping effect without the gap size distribution. Because path length is directly related to gap probability in Beer's law, a physical model was established to connect the average gap probability and the LAI using the path length distribution. The path length distribution models the clumping effect in combination with the average probability rather than calculate clumping index alone. Thus, we calculate the clumping-corrected LAI first and then the clumping index rather than use clumping index to correct LAI. The path length distribution model has the advantage of characterizing nonrandomness inside crowns caused by inconsistent path length and performs well for ground measurements [7], [8], [44]–[46]. The importance of path length was also recognized in a recent airborne lidar study, where path length correction was made to the lidar penetration rate as a correction ratio [47]. The distribution of path lengths, which models the clumping effect from a special perspective, might be useful for modeling clumping using airborne lidar. In the previous version of path length distribution model, the path length distribution was inversed from traditional gap transect data, which is not available in airborne lidar data as aforementioned. In this paper, we proposed a new approach which obtains the path length distribution directly from the 3-D information.

Through obtaining gap probability and path length distribution from airborne point cloud data, we migrated the path length distribution model on airborne lidar data to quantify the clumping effect and clumping-corrected LAI. We analyzed the data using grids of varying cell sizes and performed the further calculations in each grid cell. First, we separated the tree crown areas from large gaps in each grid cell and associated them with within-crown and between-crown areas of interest. This step was achieved by using vertical crown cover (VCC), which can be estimated to a high precision using a simple proportion of canopy points in first-return data [48]. Second, we calculated the within-crown LAI using gap probability and path length distribution of within-crown areas in each grid cell. The gap probability was estimated using laser penetration metric (LPM), also called laser penetration index derived from the vertical and horizontal distribution of hits in the areas of dense cover. The path lengths were estimated by canopy height model (CHM) which effectively measures the spatial distribution of canopy heights in each grid cell. Third, the LAI was calculated as the product of within-crown LAI and the proportion of within-crown area (VCC) in each grid cell. Finally, the LPM and LAI were validated using *in situ* measurements (Fig. 1). It should be noted that the clumping corrections of both airborne retrieval and field validation in this paper focus on between-crown and within-crown clumping beyond the shoot level, because neither airborne retrieval nor indirect field measurement can quantify the needle-to-shoot level of clumping. The correction of leaf angle distribution and woody component was not applied because this information is unavailable from airborne lidar and does not influence the validation of clumping-corrected LAI.

II. Materials

A. Study Area

The study area is located in the Genhe forest reserve (120° 12′–122° 55′ E, 50° 20′–52° 30′ N), which is at the western face of north Greater Khingan (Fig. 2). The elevations range from approximately 775 to 1300 m, and the slopes are less than 15° in 80% of the area. Located in the northernmost area of Inner Mongolia, Genhe has a monsoon-influenced subarctic climate and is officially designated the coldest city in China. The forest is mainly composed of *Larix gmelinii*

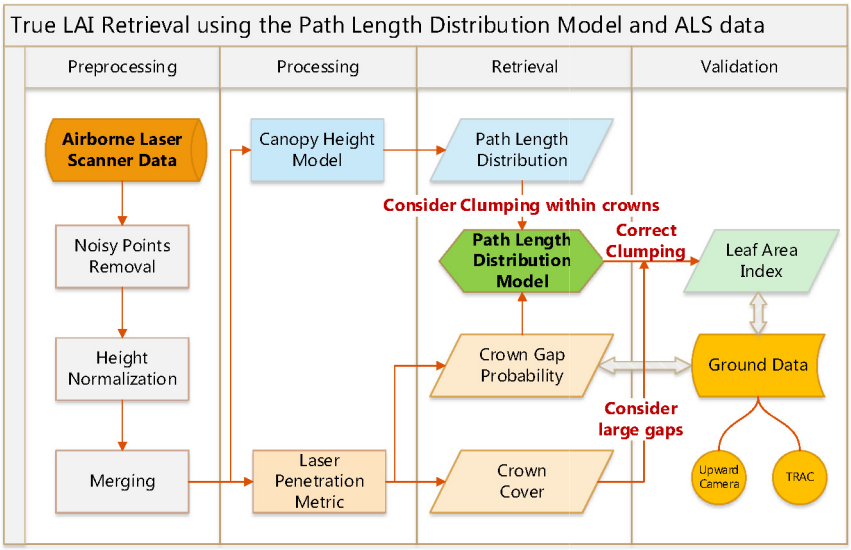

Fig. 1. Workflow diagram for estimating the clumping index and LAI by using the path length distribution model and ALS data.

(Rupr.) Rupr., *Betula platyphylla* Suk, and *Pinus sylvestris* var. *mongolica* Litv. [49].

B. Airborne Lidar Data

Airborne lidar data were collected using a Leica ALS60 system onboard a Yun-5 aircraft. This system works at a wavelength of 1064 nm and with a 0.22-mrad beam divergence. ALS60 was flown over the study area in the summer of 2012. It operated at a 166-kHz pulse rate at 1800 m above ground level with a field of view (FOV) of approximately 30°. Absolute scan angle and positions of the reflecting surfaces for each laser pulse were resolved using the range estimates from lidar, the position of the platform from global positioning system receivers, the attitude (roll, pitch, and yaw) of the lidar sensor from inertial navigation systems, and the orientation of the scanning mirror from angle encoders. Statistics of scan angles indicate that 97% of pulses falling within the 0°–12° zenith angles and 99% of pulses falling within the 0°–15° zenith angles. A maximum number of four returns were recorded per beam. The data used in this paper are a subset of 20 flight lines, covering a 5700 m × 5800 m area (Fig. 2). The average pulse density was 5.91 pulses/m^2, and the average point density was 8.24 points/m^2.

C. Field Measurements

Field campaigns were conducted in 18 plots (45 m × 45 m) of the flight area (Fig. 2), using upward photography and tracing radiation and architecture of canopies (TRAC; 3rd Wave Engineering, ON, Canada). The field campaigns of vegetation monitoring were coordinated from 2013, and then the measurements were conducted during the same period of the year as for the flight in 2012. Upward photography measurements were conducted in all 18 plots, while TRAC measurements were conducted in 13 plots, with 200- to 300-m transects in each plot. The field measurement is a part of simultaneous satellite-borne, airborne, and ground-based experiments in addition to our study of LAI, and the other five plots were specially designed for the study of terrain effects and did not have TRAC measurement due to the limitations of slope and accessibility.

The objective of this paper is to correct the clumping beyond shoot level using airborne lidar. In field measurement, we also quantified the clumping and calculate the LAI beyond the shoot level, in order to make the field data correspond to the airborne results. The needle-to-shoot level of clumping was not measured because it relies on manual measurements and is not available in airborne retrieval. Similarly, the woody components and the leaf angle distribution were not measured but considered in validation. Because the needle-to-shoot level clumping, the woody components and the leaf angle distribution have the same contribution in airborne lidar retrieval and field measurement; the missing of these information does not limit the validation of the clumping beyond shoot level and the clumping-corrected area index.

Upward photography was employed for validation mainly because it provides a zenith-direction observation, similar to the ALS data. It was also found to outperform fisheye photography when correcting for the clumping effect and estimating the LAI [50]. Approximately 50 upward photographs were taken using a Nikon D3000 in each plot along two diagonals across the sampling plot, generally under cloudy conditions, in JPEG format [51]. The original images had a size of 2592 × 3872 pixels and a viewing angle of 66.4° × 47.9°, and 60% of them were cropped to provide a viewing angle similar to that of airborne lidar. The k-means clustering method was employed to classify the images into sky and trees. Inspired by a previous work [52], the two peaks of the blue channel histogram were detected as two initial inputs of the k-means clustering method for the automatic process. The histogram was also found to be helpful for overcoming exposure issues and scattering effects [52], [53]. The total gap probability was calculated using classified images and then used for validation of the ALS gap probability. Then, the clumping effect was corrected by dividing the gap probability

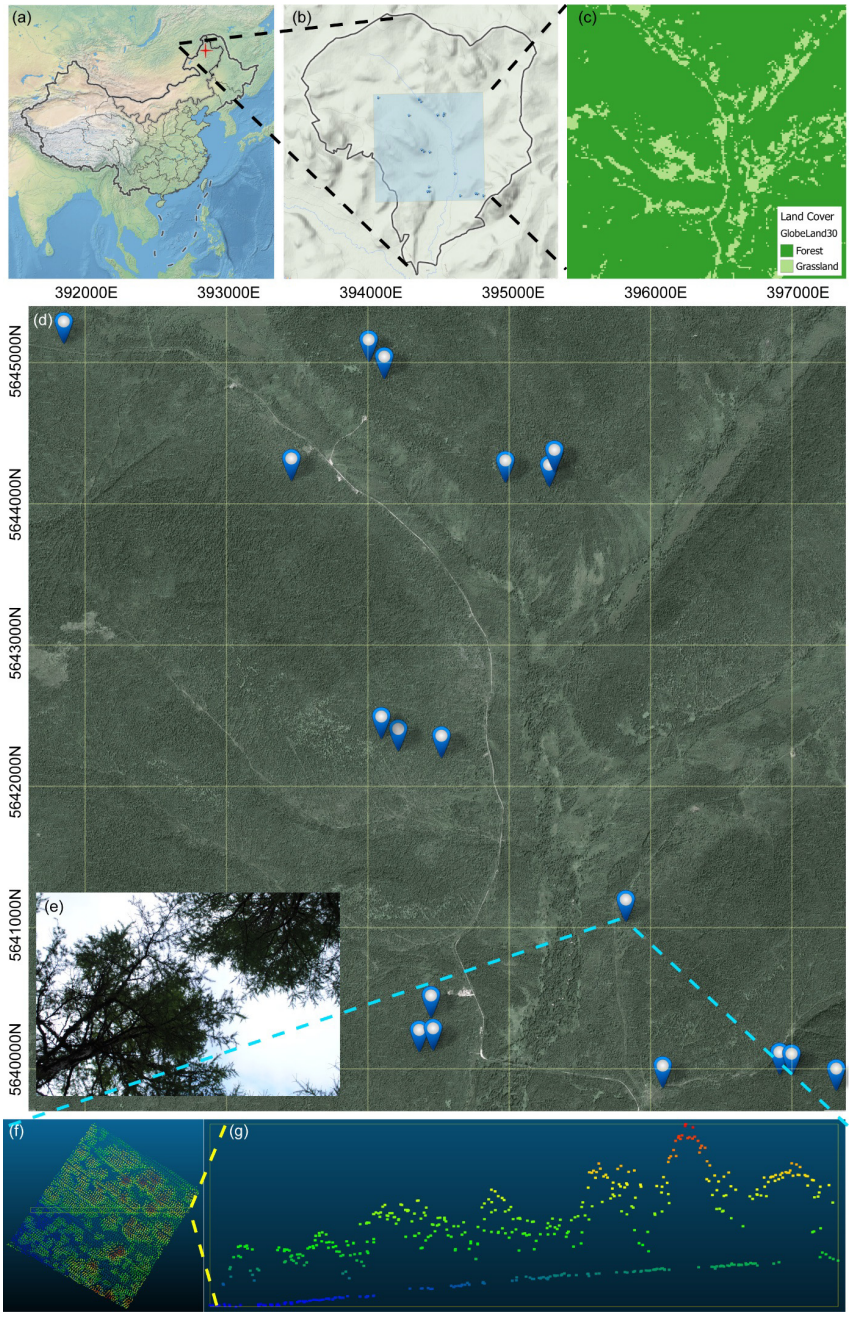

Fig. 2. ALS data area and 18 field sites in the Genhe forest reserve. (a) Position of the research area. (b) Google physical map of the research area. (c) Globeland30 land cover map of the ALS data area. (d) Google satellite map of the ALS data area and the positions of the 18 field sites. (e) Upward photography. (f) Point cloud data of site L1. (g) Transect of the point cloud data of site L1.

into between-crown and within-crown gaps, which was first proposed by Macfarlane *et al.* [50] and was then successfully applied to continuously monitor the clumping-effect-corrected LAI at the ecosystem scale [54]. After image classification, the gap transects were sampled from the classified images. For each image, several lines were sampled and combined into a long gap transect. We used an excessive sampling scheme so that all the pixels of the images were used. The large gaps between crowns were separated with a threshold of ten times the leaf width [7]. The LAIe was calculated by directly inverting Beer's law and the total gap probability. The LAI within crowns was calculated using the within-crown gap probability, and then, the LAI within crowns was multiplied by the fraction of the crown cover to calculate the LAI. A plagiophile leaf angle distribution, which was suggested to be more appropriate than a spherical distribution for temperate and boreal ecoclimatic regions [55], was used in both ground and airborne calculations, although the choice of leaf angle distribution does not influence the validation of clumping correction. The use of leaf angle distribution will be discussed in Section V-E.

As both the leafy component and woody component contribute to the ALS echo, the results of ALS data generally represent the plant area index (PAI), which includes all the components of the plants. To match the results of the ALS data, the same classification was adopted in processing the

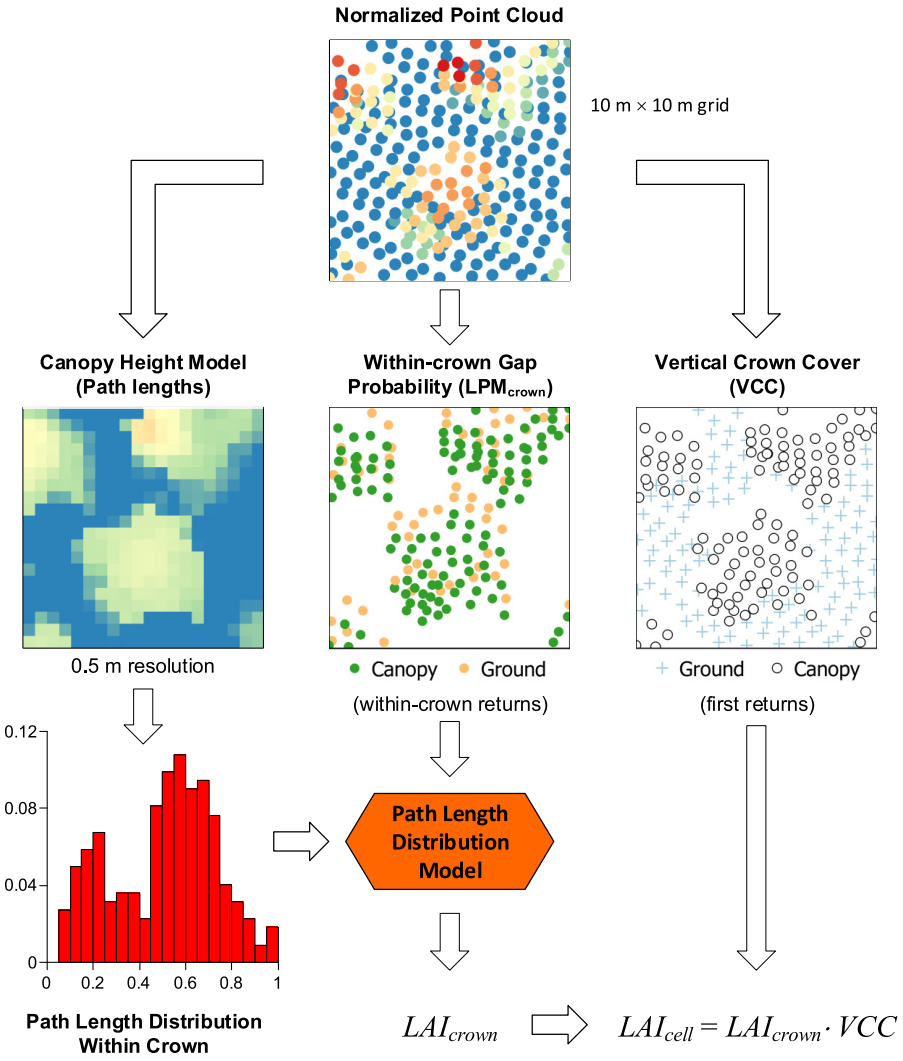

Fig. 3. Workflow diagram for processing the normalized point cloud data and calculating the LAI for each grid cell.

photographs. The photographs were classified into the following two components: those of the sky and those of plants.

III. Methods

A. Preprocessing

The airborne lidar data were preprocessed using the lasnoise, lasmerge, lastile, and lasground modules of LAStools [56]. First, the lasnoise module was used in each flight line to remove noise points (isolated points in the sky for example). Second, the lasmerge module was used to merge the flight lines together. Third, the lasground module was used to extract the ground points and then calculate the relative height above the ground for each point [57]. Because the ALS60 data set for the whole research area is too big to execute the lasground module, the data were split into 1000 m × 1000 m tiles with a 50-m buffer in each direction using the lastile module. The lasground module was applied to each tile, and the results were merged with the buffer removed. The buffer was used to avoid using the results at the edge of the data. Then, the height normalized ALS data were obtained for future processing. With a height threshold, points were classified as canopy and ground returns. The height threshold was set as 1 m to exclude the low grass and retain the relatively high underlying vegetation. Since all these preprocesses are commonly used in the lidar community, they could thus be achieved easily by using the batch-scriptable and friendly software LAStools or other similar tools or libraries.

B. Gridding

For LAI mapping, the 3-D height normalized ALS data were gridded into an image. Grids with sizes of 5, 10, 30, 50, 100, 250, and 500 m were tested in this paper. The LAI was retrieved for each grid cell. For each grid cell, two lidar metrics and a path length distribution were calculated for LAI retrieval (Fig. 3).

C. Theoretical Basis: Path Length Distribution Model

The path length distribution model was proposed by Hu *et al.* [7] to address the clumping effect between crowns and the crown shape-induced nonrandomness within crowns. It is based on the theoretical prototype of Beer's law and the path length distribution within crowns. The model is ideal for lidar, as it is able to take advantage of the 3-D point cloud information of lidar data, and is thus able to provide path

lengths directly, rather than via the traditional detailed gap distribution, which is inaccessible for large-footprint lidar data.

The path length distribution, which is used to consider the nonrandomness, is defined as the probability density function of a specific path length

$$p_{\mathrm{lr}}(\mathrm{lr}) = \frac{\hat{p}_{\mathrm{lr}}(\mathrm{lr})}{\int_0^1 \hat{p}_{\mathrm{lr}}(\mathrm{lr}) d(\mathrm{lr})} \quad (1)$$

$$\mathrm{lr} = l / l_{\max} \quad (2)$$

where lr is the relative path length normalized to [0, 1], l is the absolute path length at a location of transect, and $l_{\max}$ is the maximum path length along the transect. $\hat{p}_{\mathrm{lr}}(\mathrm{lr})$ is the frequency of lr falling within the infinitesimal interval [lr, lr + d(lr)].

The LAI of the path length distribution model can be expressed as

$$\mathrm{LAI\_PATH}_{\mathrm{crown}} = \int_0^1 (\mathrm{FAVD} \cdot l_{\max}) \cdot lr \cdot p_{\mathrm{lr}}(\mathrm{lr}) d(\mathrm{lr}) \quad (3)$$

where FAVD is the foliage area volume density. The intermediate variables FAVD $\times$ $l_{\max}$ can be retrieved by solving

$$\overline{P_{\mathrm{crown}}(\theta)} = \int_0^1 e^{-G \cdot (\mathrm{FAVD} \cdot l_{\max}) \cdot lr} \cdot p_{\mathrm{lr}}(\mathrm{lr}) d(\mathrm{lr}) \quad (4)$$

where $\overline{P(\theta)}$ is the within-crown gap probability of each grid cell, and G is the leaf projection coefficient which can be calculated from leaf angle distribution [58].

Equations (3) and (4) of path length distribution are mainly used to correct clumping within crowns, and their results are clumping-corrected LAI within crowns ($\mathrm{LAI\_PATH}_{\mathrm{crown}}$). Only two inputs are needed for (3) and (4): the average gap probability within crowns [$\overline{P_{\mathrm{crown}}(\theta)}$] and the path length distribution within crowns [p_{lr}(lr)]. The clumping between crowns was corrected by fraction of large gaps in path length distribution model. All the calculations were made grid cell by grid cell. For each grid cell, the fraction of large gaps and the average within-crown gap probability were obtained from two LPMs, while the path length distribution was obtained from the path lengths from the CHM based on statistics.

D. Gap Probability From Lidar Metrics

Two lidar metrics were calculated and combined for the LAI estimation in each grid cell. Within-crown gap probability was used to estimate the LAI within crowns ($\mathrm{LAI}_{\mathrm{crown}}$) in combination with path length distribution within crowns. VCC, which is the proportion of tree crowns, ignoring within-crown gaps [48], [59], was used to quantify large gaps between crowns (i.e., correct horizontal clumping) and to convert the $\mathrm{LAI}_{\mathrm{crown}}$ to the LAI of the grid cell

$$\mathrm{LAI}_{\mathrm{cell}} = \mathrm{LAI}_{\mathrm{crown}} \cdot \mathrm{VCC}. \quad (5)$$

The relationship between the total gap probability (P_{cell}), within-crown gap probability (P_{crown}), and VCC is

$$P_{\mathrm{cell}} = (1 - \mathrm{VCC}) + P_{\mathrm{crown}} \cdot \mathrm{VCC} \quad (6)$$

where 1 $-$ VCC is the between-crown gap probability.

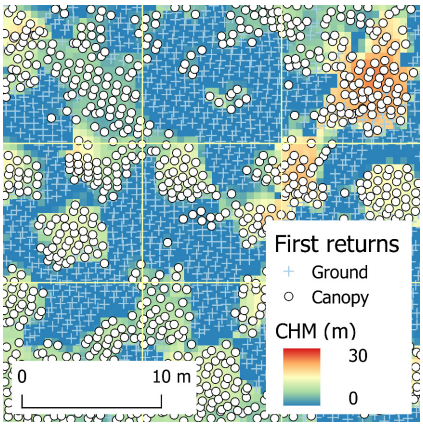

Fig. 4. VCC from first-return proportion.

1) Vertical Crown Cover (VCC): VCC was calculated to quantify the proportion of tree crowns in each grid cell. First, a height threshold of 3 m was used to determine whether the grid has trees. If a grid cell contains no point higher than 3 m, it is regarded as a "no-tree" grid cell; otherwise, it is regarded as a "tree" grid cell.

For a "no-tree" grid cell, the VCC is not calculated and all points of the grid cell are used for calculating $\mathrm{LAI}_{\mathrm{cell}}$ using the path length distribution model (Section III-E).

For a "tree" grid cell, the VCC values are calculated as the crown proportions of first returns (Fig. 4)

$$\mathrm{VCC} = N_{\mathrm{first\_canopy}} / N_{\mathrm{first}} \quad (7)$$

where $N_{\mathrm{firs\_canopy}}$ is the number of first returns classified as canopy and N_{first} is the total number of first returns. Fig. 4 shows nine grid cells in the grid and the analysis with the grid cells.

Then, only the returns from tree crowns are used to calculate the $\mathrm{LAI}_{\mathrm{crown}}$ using the path length distribution model, and the $\mathrm{LAI}_{\mathrm{cell}}$ is calculated by multiplying the $\mathrm{LAI}_{\mathrm{crown}}$ with the VCC [see (5)].

It is reasonable to calculate the VCC using the first returns of ALS, as the ALS footprint is generally larger than gaps within a tree crown. It is convenient to distinguish and calculate the proportions of tree crowns and large gaps between crowns because the first returns from a crown are always canopy returns, and the first returns from large gaps between crowns are always ground returns. In this paper, the ALS footprint had a diameter of 0.4 m, and there were rarely big holes larger than 0.4 m within crowns in the vertical direction; thus, a laser pulse could hardly pass through the canopy without any contact and hit the ground as the first return along the vertical direction.

The resolution of VCC is determined by point density to ensure there are enough laser pulses in a grid cell. Considering that the VCC measurement using ALS is like a systematic sampling, the accuracy of VCC calculation is mainly influenced by the number of laser pulses in each grid, which is similar as sampling number. In this paper, the VCC was calculated using ALS data with an average point density of 5.91 pulses/m^2 and an average spacing of 0.41 m, which meets the average spacing requirement of 1 m suggested in [48]. The

TABLE I
REPRESENTATIVE LPMS

LPM	Canopy Cover = 1 - LPM
$LPM_{all} = \frac{N_{ground}}{N}$	$ACI = \frac{N_{canopy}}{N}$
$LPM_{first} = \frac{N_{single\_ground} + N_{first\_ground}}{N_{single} + N_{first}}$	$FCI = \frac{N_{single\_canopy} + N_{first\_canopy}}{N_{single} + N_{first}}$
$LPM_{last} = \frac{N_{single\_ground} + N_{last\_ground}}{N_{single} + N_{last}}$	$LCI = \frac{N_{single\_canopy} + N_{last\_canopy}}{N_{single} + N_{last}}$
$LPM_{Solberg} = \frac{N_{single\_ground} + 0.5\left(N_{first\_ground} + N_{last\_ground}\right)}{N_{single} + 0.5\left(N_{first} + N_{last}\right)}$	$SCI = \frac{N_{single\_canopy} + 0.5\left(N_{first\_canopy} + N_{last\_canopy}\right)}{N_{single} + 0.5\left(N_{first} + N_{last}\right)}$

N - number of all returns, N_{ground} - number of ground returns, N_{canopy} - number of canopy returns, N_{first} - number of first returns, N_{last} - number of last returns, N_{single} - number of single returns, N_{first_ground} - number of first returns classified as ground, N_{last_ground} - number of last returns classified as ground, N_{single_ground} - number of single returns classified as ground, N_{first_canopy} - number of first returns classified as canopy, N_{last_canopy} - number of last returns classified as canopy, N_{single_canopy} - number of single returns classified as canopy, ACI – all echo cover index, FCI – first echo cover index, LCI – last echo cover index, SCI – Solberg's cover index.

minimum grid size was set as 5 m considering there are on average 148 laser pulses in each grid cell (yielding a VCC precision of better than 0.01).

2) Within-Crown Gap Probability From the LPM (for the LAI_{crown}): After excluding the ground returns between crowns in each grid cell, the LPM was calculated as a proxy of within-crown gap probability. It is not easy to clearly define the gap probability because airborne lidar has finite-sized footprints. Several LPMs have been constructed (Table I), with only first returns, only last returns, all returns, or a combination of first and last returns [27], [48], [60]. Field validations showed that using only first returns will underestimate the gap probability, while using only last returns will overestimate the gap probability [27], [48]. In this paper, four LPMs (Table I) were calculated and compared.

E. LAI From the Path Length Distribution Model

The path length of each laser pulse is not known locally because lidar returns are always vertically inside the tree crowns rather than in the envelope of tree crowns. Therefore, we proposed to use a high-resolution CHM to represent the upper envelope of tree crowns. The CHM was generated as a proxy of the path length distribution, as path length is the distance covered when traveling through the canopies.

A pit-free CHM was generated via a multilevel method that combines the partial CHMs generated with points above certain heights [61]. This process can be achieved with a script using the lastile, lasthin, blast2dem, and lasgrid modules of LAStools [56]. With an average point density of 5.91 pulses/m^2 and an average spacing of 0.41 m, the pit-free CHM was generated with a resolution of 0.5 m.

Then, the path length distribution was obtained from the pit-free CHM in each grid cell based on statistics. Grids with sizes of 5, 10, 30, 50, 100, 250, and 500 m were tested in this paper. The minimum grid size was set as 5 m to take the representativeness and statistical requirements of the gap probability and path length distribution into consideration. In a 5-m grid cell, there were on average 206 points (yielding a gap probability precision of better than 0.005) and 100 path lengths. Only the CHM in the crown area was used.

The LAI was retrieved for each grid (Fig. 3). First, the VCC, within-crown gap probability, and within-crown path lengths were calculated for each grid cell. Second, the within-crown gap probability and within-crown path lengths were input into the path length distribution model to retrieve the $\mathrm{LAI}_{\mathrm{crown}}$ [see (3) and (4)]. Finally, the LAI of each grid cell was calculated by multiplying by the VCC [see (5)].

F. Clumping

The LAIs and clumping indices were calculated for analyzing the clumping effect in different scales. All these clumping indices and LAIe are directional quantities, and were in the near-vertical direction in this paper.

First, the LAIe of each grid cell was calculated by directly inverting Beer's law to the total gap probability (P_{cell}) for each grid cell

$$\mathrm{LAI}_e = -\ln(P_{\mathrm{cell}})/G. \tag{8}$$

Then, the total clumping index was calculated conveniently based on its definition

$$\Omega_{\mathrm{All}} = \mathrm{LAI}_e/\mathrm{LAI}_{\mathrm{cell}} \tag{9}$$

where the $\mathrm{LAI}_{\mathrm{cell}}$, defined in (5), is the result of our method (Fig. 3) and takes into consideration both the between-crown clumping by the VCC and the within-crown clumping by the path length distribution model [$\mathrm{LAI}_{\mathrm{crown}}$, see (3)].

In addition, we defined an LAI_e_VCC between the LAI_e and LAI and two clumping indices were used here to represent different sources of the clumping effect. The LAI_e_VCC, which considers the between-crown clumping by the VCC but

does not consider the within-crown clumping, is defined as the product of the effective LAI within crowns and the VCC

$$\mathrm{LAI}_e\_\mathrm{VCC} = -\ln(P_{\mathrm{crown}})/G \cdot VCC. \tag{10}$$

The LAI_e, LAI_e_VCC, and $\mathrm{LAI}_{\mathrm{cell}}$ are all values in each grid cell and have different degrees of clumping. We split the total clumping into two parts

$$\Omega_{\mathrm{VCC}} = \mathrm{LAI}_e/\mathrm{LAI}_e\_\mathrm{VCC} \tag{11}$$

$$\Omega_{\mathrm{PATH}} = \mathrm{LAI}_e\_\mathrm{VCC}/\mathrm{LAI}_{\mathrm{cell}} \tag{12}$$

where Ω_{VCC} represents the clumping effect between crowns; the difference between LAI_e and LAI_e_VCC is due to the between-crown clumping, which is dominated by the VCC; and Ω_{PATH} represents the clumping effect within crowns; the difference between LAI_e_VCC and LAI is due to the within-crown clumping, which is caused by the heterogeneous spatial distribution of vertical leaf profile and can be eliminated by the path length distribution model.

IV. Results

A. Gap Probability From Laser Penetration Metric (LPM)

Several LPMs were validated using field photography (Fig. 5). The total gap probabilities from the LPM for each grid cell were calculated for comparison with the field data.

The results show that $\mathrm{LPM}_{\mathrm{all}}$ and $\mathrm{LPM}_{\mathrm{Solberg}}$ perform the best against the field data, with an RMSE of 0.07. $\mathrm{LPM}_{\mathrm{first}}$ is generally lower than the field gap fraction, while $\mathrm{LPM}_{\mathrm{last}}$ is higher than the field gap fraction. Their trends and accuracy are consistent with those in [28] and [48].

The underestimation of $\mathrm{LPM}_{\mathrm{first}}$ and overestimation of $\mathrm{LPM}_{\mathrm{last}}$ are understandable because certain laser pulses hitting canopies have canopy echoes as first returns and ground echoes as last returns, due to the large footprints. When a pulse has both canopy and ground returns, its footprint is occupied partly by the canopy and partly by the ground, rather than being pure canopy or pure ground. $\mathrm{LPM}_{\mathrm{first}}$ regards these mixed areas as pure canopy and thus underestimates the fraction of ground, while $\mathrm{LPM}_{\mathrm{last}}$ regards these mixed areas as pure ground and thus overestimates the fraction of ground. Both $\mathrm{LPM}_{\mathrm{all}}$ and $\mathrm{LPM}_{\mathrm{Solberg}}$ utilize first and last returns, thus balancing the contributions of first and last returns. The difference between $\mathrm{LPM}_{\mathrm{all}}$ and $\mathrm{LPM}_{\mathrm{Solberg}}$ is very small, although $\mathrm{LPM}_{\mathrm{all}}$ also utilizes the intermediate returns. This is because the proportion of intermediate returns is very small, being only 3.7%, 3.7%, and 5.7% of that of the first, last, and single returns, respectively.

The results show that both $\mathrm{LPM}_{\mathrm{all}}$ and $\mathrm{LPM}_{\mathrm{Solberg}}$ are capable of representing gap probability well and have very little difference; thus, $\mathrm{LPM}_{\mathrm{all}}$ can be used for further processing.

B. Path Length From Canopy Height Model (CHM)

The CHM was generated with a resolution of 0.5 m (Fig. 6). In total, 99.9% of pixels in the research area have a height of less than 30 m. The rivers, roads, and channels appear clearly on the map, with heights of approximately 0 m. Some traces of tree rotation can also be found, for example, in the bottom left part of the image. Tall trees are generally distributed deep

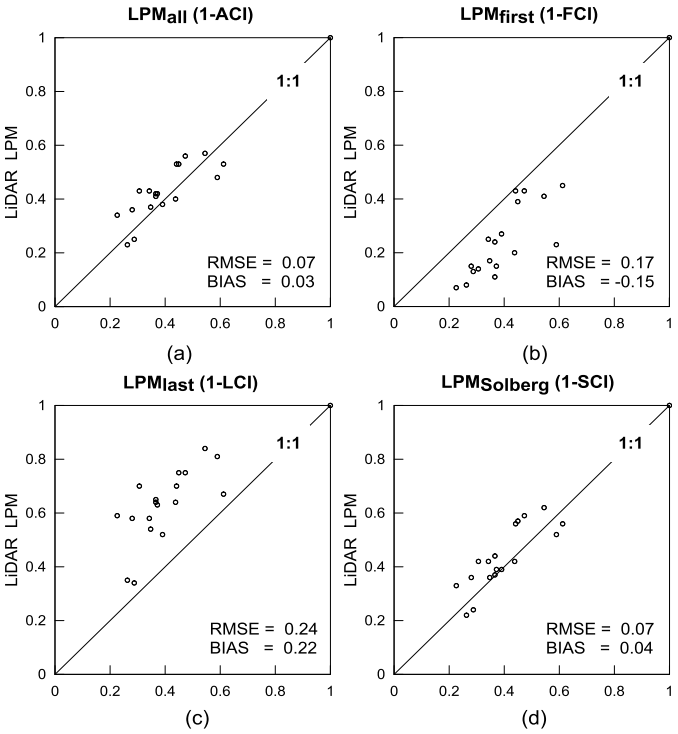

Fig. 5. Validation of the LPMs using field photography. (a) LPM calculated with all returns. (b) LPM calculated with only first returns. (c) LPM calculated with only last returns. (d) Solberg's LPM calculated with first and last returns.

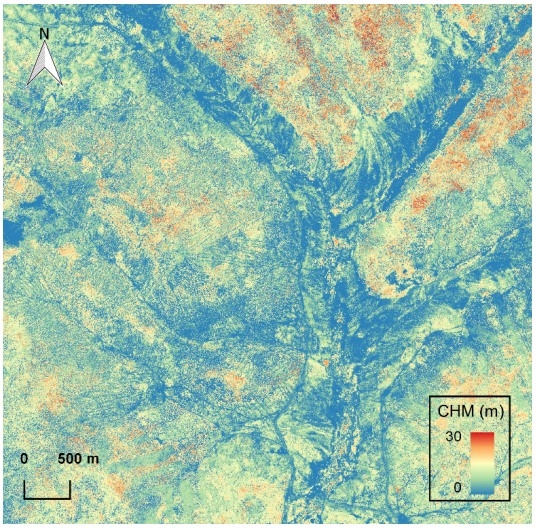

Fig. 6. Pit-free CHM generated with a 0.5-m resolution using the ALS data.

in the mountains. The results show that the CHM is able to well characterize the upper envelope of the forest. As the ALS data are near nadir, with the scanning zenith generally less than 12° and a cosine larger than 0.978, the influence of the zenith angle is lower than 3%. Thus, the vertical height of the CHM is used as the path length of the laser pulse.

C. LAI

The LAI was generated using the LPMs and CHM in the path length distribution model (Fig. 7). The largest LAI was mainly distributed in dense forests in the mountains and in a forest-grassland transition zones. According to our field survey, we found that there is better underlying vegetation in

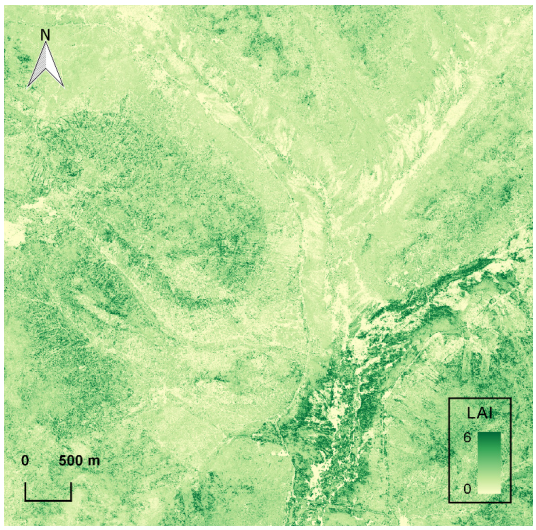

Fig. 7. LAI generated with a 5-m resolution using the ALS data using the path length distribution model.

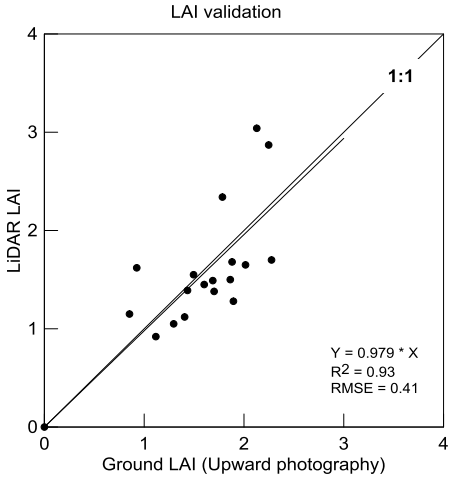

Fig. 8. Field validation of the LAI from the ALS data using the path length distribution model.

the forest-grassland transition zones due to better lighting and watering. Meanwhile, in dense forests, most light is generally blocked by the trees, and there is less water in the mountains than in the forest-grassland transition zones near a river. In the forest-grassland transition zones near a river, the underlying vegetation is generally very dense and nearly 2 m in height, and the gap probability is much lower than that in the forests. In addition, there are also some trees in the forest-grassland transition zones, although not as many as in the forests. These trees and well-grown underlying vegetation lead to a high LAI in these areas.

ALS LAIs from the path length distribution model generally characterize the clumping-corrected LAIs, with an RMSE of 0.41 (Fig. 8). The ALS LAIs of most sites are in good agreement with the field measurements, with a difference of less than 0.5, while a difference from 0.5 to 1 was found in several plots, which is not as good as expected. These differences might come from the differences in the mechanism and resolution between the ALS data and the upward camera. The pattern of LAI validation is similar to that of the LPM validation (Fig. 5) and will be discussed in Section V. A similar large error was also found in previous ALS studies of the LAIe estimation [26], [47], [48].

The LAIs of different resolutions were compared, and the results are generally consistent, especially when the LAI and the pixel size are not very large (Fig. 9). The LAIs of different resolutions are aggregated to 500-m pixels for comparisons. The average differences of all pixels are less than 5% from 5- to 250-m resolutions [Fig. 9(a)–(e)] and 6% between 5- and 500-m resolutions [Fig. 9(f)]. The differences become larger when larger resolutions are compared. This could occur because the variation of FAVD becomes greater for larger pixels. The consistency indicates that implementation of the path length distribution model on ALS data is not sensitive to the resolution. Note that the 5-m-resolution data already have enough cloud points and path length distribution information for statistics for each grid cell, which is a requirement for obtaining reasonable results.

V. Discussion

A. Clumping Index at Different Scales

Three maps of the clumping index were then calculated to analyze the spatial pattern of the clumping effect at different scales. The clumping index between crowns Ω_{VCC} [Fig. 10(b)] contributes the most information to the spatial pattern of the total clumping index Ω_{ALL} [Fig. 10(a)], while the clumping index within crowns Ω_{PATH} [Fig. 10(c)] is more homogeneous spatially. This phenomenon is understandable, as the between-crown clumping is more related to the spatial distribution of canopies and the large gaps between crowns, while the within-crown clumping is more related to the shape of the tree crowns. The between-crown clumping map [Fig. 10(b)] is visually correlated with the CHM map (Fig. 6), because the between-crown clumping is calculated based on VCC, which is the proportion of areas higher than a height threshold and is related to CHM. The areas with continuously large canopy heights are dense forests which have more trees and smaller gaps between the crowns, resulting in a smaller VCC and a larger clumping index. The areas with low canopy heights have fewer trees and greater gaps between the crowns and thus are more clumped and have a smaller between-crown clumping index. The difference in the within-crown clumping index between the different land covers is less obvious [Fig. 10(c)], indicating the between-crown clumping contributes most of the spatial variance and the two clumping indices are well separated. The between-crown clumping is influenced by the density and size of trees, which vary with different species and even different locations of the same species. The within-crown clumping is influenced by the collective effect of the crown shape and the leaf area density within crowns, which might vary with different species. The within-crown clumping is less variable because the variance of crown shape and leaf area density is generally smaller than that of the tree density.

B. Validity of Correcting Clumping Effect Using the Path Length Distribution Model

The ALS clumping index was compared with field measurement (Table II). The ALS clumping index generally agrees

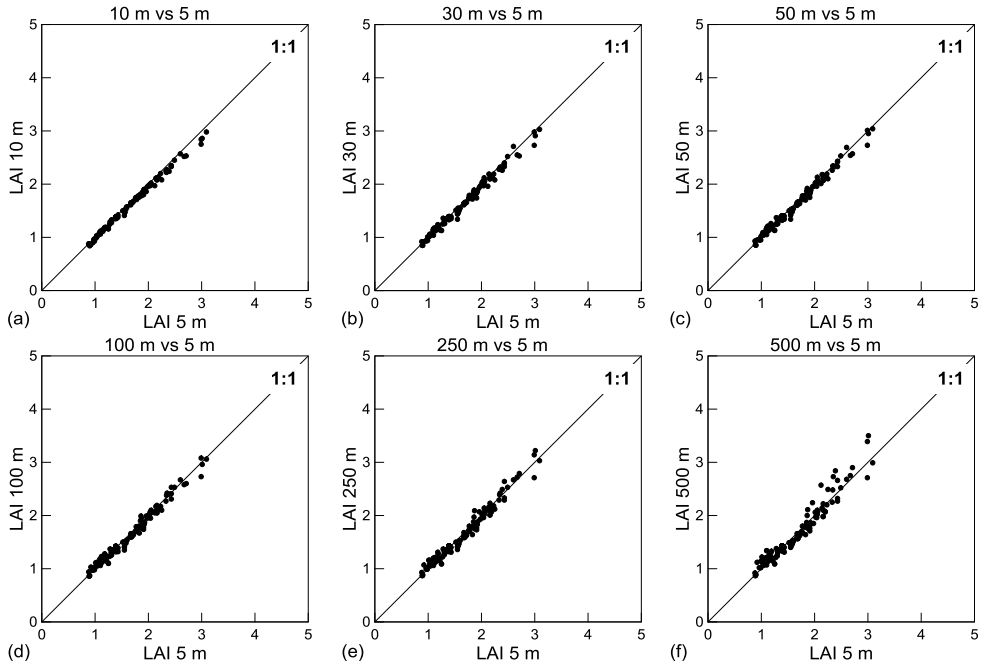

Fig. 9. Comparison of the LAIs with different resolutions. The LAIs of different resolutions are aggregated to 500-m pixels for comparison.

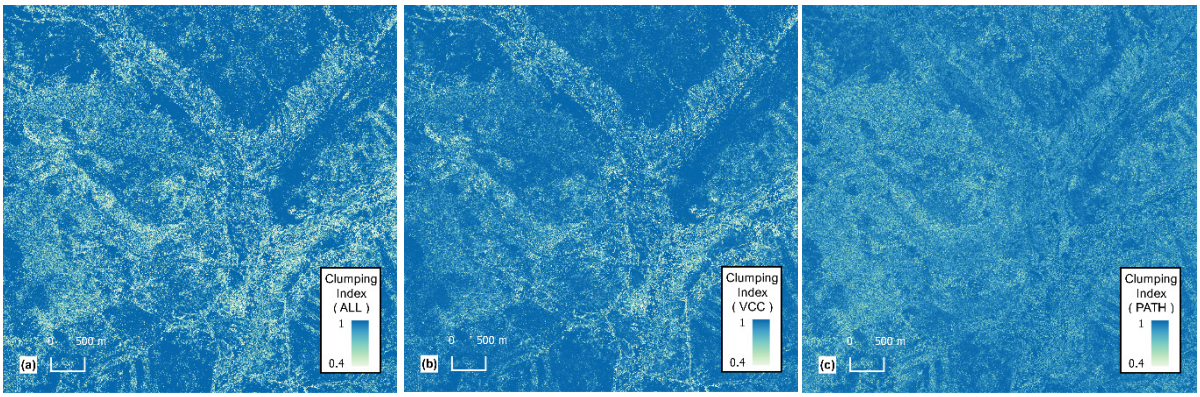

Fig. 10. Clumping index maps at different scales. (a) Clumping index in total. (b) Clumping index between crowns. (c) Clumping index within crowns.

with that of the field measurement, with an average difference of approximately 0.05. This difference is not large, since there is also a difference of 0.04 between field photography and TRAC measurement. These differences might mainly come from the differences in data acquisition mechanism between the ALS and the field measurements, which result in different input data at different resolutions. The difference in the LAIe, which comes from the gap probability [Fig. 5(a)], also propagated to the clumping index, because the LAIe is the numerator for calculating clumping index. There are observation towers for other instruments installed in some sites, which might have more influences on the field observations on large zenith angle than the near-nadir ALS measurement. Differences between the mechanisms of the ALS and upward camera do exist and are another source of the differences in validation. In addition, some of the field sites are on a sloping terrain with a slope of approximately 15°; thus, the slope effect might also bring some uncertainties to the field measurements and validation.

The main advantage of using the path length distribution is that it is a physical model utilizing the advantage of 3-D information while avoiding the disadvantage of identifying small gaps with large-footprint ALS data. The path length distribution model itself does not have many parameters to adjust and is thus convenient and comparable for application. The consistency between the results at different resolutions also demonstrates its stability and potential for application.

C. Accuracy of the LPM as a Proxy of Gap Probability

The LPM data are an important data source for the LAI estimation. The pattern of the LAI validation (Fig. 8) is similar to that of the LPM validation [Fig. 5(a)].

There are still some differences in mechanism and resolution. First, the upward camera has a much higher resolution (higher than 0.01 m), which can be used to quantify the proportion of sky and trees more precisely, while the ALS has a much larger footprint (0.4 m). Second, their coverages

TABLE II
CLUMPING INDEX OF ALS, FIELD PHOTOGRAPHY, AND TRAC IN 18 FIELD SITES. TRAC MEASUREMENTS WERE MADE ON 13 SITES

Clumping Index	ALS	Photography	TRAC
L1	0.89	0.86	0.88
L2	0.92	0.84	0.95
L3	0.93	0.92	0.92
L4	0.98	0.98	0.93
L5	0.99	0.93	0.92
L6	0.97	0.93	0.88
L7	0.69	0.79	0.81
L8	0.94	0.85	0.88
L9	0.98	0.88	0.94
A1	0.78	0.87	-
A2	0.87	0.89	-
A3	0.93	0.82	-
A4	0.96	0.94	0.93
A5	0.84	0.85	-
A6	0.75	0.79	-
A7	0.96	0.81	0.89
A8	0.90	0.86	0.95
A9	0.95	0.89	0.92

are also different; the ALS generally has a full coverage of the whole plot, with hundreds of large footprints, while the upward photographs cover parts of the plot, especially after cropping. The upward photography and downward LPM are equally limited, but their agreement is comforting. Thus, there are still some differences between the LPM of ALS and the gap probability of upward photography [Fig. 5(a)]; these differences further propagate to the LAI (Fig. 8). There is a maximum error of 0.13 in gap probability [Fig. 5(a)], which results in a maximum error of 0.8 in LAIe and will be further magnified after considering the clumping.

The use of small-footprint and high-density data should be helpful for better characterizing gap probability, as the canopy and ground returns will be less mixed and there will be more returns in each grid cell.

D. Accuracy of CHM as a Proxy of Path Length Distribution

The height in each grid cell was used as the path length in this paper due to the limitations of the ALS footprint and point density. The CHM is able to characterize the relative path length distribution roughly, while there are still some differences. The returns at the top of the canopies and the ground are the most complete and informative and thus were used to extract the path length distribution in this paper. Although we believe that the relative ratios of the path lengths are similar, the use of heights will underestimate the changes in path lengths. The impact of the CHM will be reduced by the VCC, as path length modeling is only used for correcting the clumping effect within crowns.

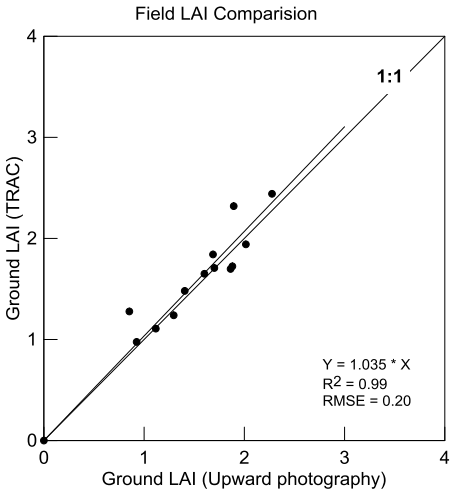

Fig. 11. Comparison of LAI using two field-based methods.

Extracting the lower envelope of the canopies in the ALS point data is difficult due to the much lower point density in the lower part of the canopies. In addition, the ALS pulses do not always have returns exactly within the lower boundary of the canopies. The waveform data might have the potential for extracting a more accurate path length, as the lower envelope is clearer in the waveform profile. Alternative methods, such as the cloth simulation filter [62], could also be tested for extracting ground points.

E. Matching Lidar and Field Measurements

Matching lidar and field measurements is important for comparison due to the variety in observation angles, projected areas, and LAI definitions.

Matching the observation angle is necessary when comparing the gap probability, as the gap probability changes with the zenith angle even in a homogenous scene due to the change in path length. The ALS data generally have small observation angles, while some field instruments, such as LAI-2000, Fisheye camera, and TRAC, have larger observation zenith angles or wider FOVs. In this paper, only upward photography was used for gap probability validation after being cropped to an FOV similar to that of ALS. Both TRAC and upward photography were used for correcting clumping effect, and the results show that the final LAI validation with upward photography (RMSE $=$ 0.41) is slightly better than that with TRAC (RMSE $=$ 0.45). It is not a question of which instrument is better, because these two sets of data generally agree with each other well (Fig. 11), but more whether the viewing direction and FOV of the ALS and upward photography match better. The use of the near-vertical gap probability in field measurements was also highlighted in several previous studies, and their results showed that using a smaller zenith angle close to the ALS data produced better results [48], [60]. Considering the observation angle of airborne lidar is also important, because sometimes the airborne lidar collects data without an accurate gyro stabilizer, especially in a small aircraft or an unmanned aerial vehicle.

The aircraft attitude can propagate to the laser pulse and enlarge the observation zenith. We recommend a small FOV for ALS acquisition to maintain the consistency of observation angle and data processing.

The LAI was used for the final validation because the LAI is defined vertically and thus has fewer problems in matching the observation zenith angles, as the change in path length caused by the observation angle has been considered in the LAI calculation with a cosine correction. The gap probability at different angles was converted into the LAI for different representative areas.

Matching the LAI definition was also considered in this comparison. The same basic theory, same viewing angle, and same classification were adopted in processing the ALS and photography data to reduce the uncertainties in comparison. They are comparable and enough for clumping validation because both the results of the ALS and upward photography data are clumping-corrected area index without considering woody component, G function, and needle-to-shoot area ratio. Because the leafy component and woody component are not distinguishable in both the ALS and upward photography data, the results of both the ALS and upward photography consist of the contribution of all plant components and thus represent the PAI for both. In addition, their G functions are also the same, as the ALS and upward photography have similar viewing angles. Since Beer's law-based method was used for both the ALS and upward photography, the G function has the same contribution and does not influence the comparison.

VI. Conclusion

We present a grid cell method based on path length distribution model to calculate the clumping-corrected LAI using the ALS data independently without additional measurements. Various useful and practical indicators, including ALS-derived gap probability and crown cover from laser penetration indices and path length distribution from local canopy height distribution, were brought together to comprehensively model the clumping effect and LAI.

Both the between-crown and within-crown clumping effects are corrected. The between-crown clumping is corrected by separating the within- and between-crown areas, and the within-crown clumping is corrected by using path length distribution as estimated by local canopy height distribution to consider the 3-D foliage profile. The main advantage of using the path length distribution is that it is a physical model utilizing the advantage of 3-D information while avoiding the disadvantage of identifying small gaps with large-footprint ALS data.

The lidar gap probability and path length distribution are the main inputs and main factors influencing the LAI estimation accuracy. The LPM and CHM were used as proxies of the gap probability and path length distribution, respectively. The LPM that uses both first and last returns provides a more reasonable estimation of gap probability. The CHM roughly characterizes the change in path lengths, while might slightly underestimate their magnitudes.

Limited field data show that the results are promising and a multilevel clumping analysis is consistent with the landscape flown. With the 0.4-m-footprint ALS data in this paper, the results show that the path length distribution model is capable of characterizing the clumping-corrected LAI robustly and rapidly in a large area. The ALS LAIs of different resolutions are consistent, with a difference of less than 5% from 5- to 250-m resolutions. The path length distribution model itself does not have many parameters to adjust and is thus convenient and comparable for application. Due to its consistency with the resolution and its simple configuration, the method provides an opportunity to map the clumping-corrected LAI operationally and to strengthen the ability of airborne lidar to validate the remote sensing products and to monitor vegetation changes. This grid cell method based on path length distribution is worth further testing and application using more recent laser technology.

Acknowledgment

The authors thank Dr. Z. Li, Dr. E. Chen, Dr. Q. Liu, K. Hu, M. Li, X. Mu, and colleagues of the Research Institute of Forest Resource Information Techniques, Chinese Academy of Forestry, Beijing, China, for collecting and providing the airborne lidar data. They also thank the anonymous reviewers for their helpful and valuable comments.

References

[1] G. P. Asner, J. M. O. Scurlock, and J. A. Hicke, "Global synthesis of leaf area index observations: Implications for ecological and remote sensing studies," *Global Ecol. Biogeogr.*, vol. 12, no. 3, pp. 191–205, May 2003.

[2] I. Jonckheere *et al.*, "Review of methods for *in situ* leaf area index determination: Part I. Theories, sensors and hemispherical photography," *Agricult. Forest Meteorol.*, vol. 121, pp. 19–35, Jan. 2004.

[3] S. C. Stark *et al.*, "Amazon forest carbon dynamics predicted by profiles of canopy leaf area and light environment," *Ecol. Lett.*, vol. 15, no. 12, pp. 1406–1414, Dec. 2012.

[4] GCOS, *Systematic Observation Requirements for Satellite-Based Products for Climate Supplemental Details to the Satellite-Based Component of the Implementation Plan for the Global Observing System for Climate in Support of the UNFCCC—2011 Update, Supplemental Details to the Satellite-Based Component of the Implementation Plan for the Global Observing System for Climate in Support of the UNFCCC (2010 Update)*, World Meteorol. Org., Geneva, Switzerland, 2011, p. 138.

[5] Y. Tian *et al.*, "Exploring scale-dependent ecohydrological responses in a large endorheic river basin through integrated surface water-groundwater modeling," *Water Resour. Res.*, vol. 51, no. 6, pp. 4065–4085, Jun. 2015.

[6] W. Fan, Y. Liu, X. Xu, G. Chen, and B. Zhang, "A new FAPAR analytical model based on the law of energy conservation: A case study in China," *IEEE J. Sel. Topics Appl. Earth Observ. Remote Sens.*, vol. 7, no. 9, pp. 3945–3955, Sep. 2014.

[7] R. Hu, G. Yan, X. Mu, and J. Luo, "Indirect measurement of leaf area index on the basis of path length distribution," *Remote Sens. Environ.*, vol. 155, pp. 239–247, Dec. 2014.

[8] G. Yan *et al.*, "Scale effect in indirect measurement of leaf area index," *IEEE Trans. Geosci. Remote Sens.*, vol. 54, no. 6, pp. 3475–3484, Jun. 2016.

[9] J. M. Chen, "Optically-based methods for measuring seasonal variation of leaf area index in boreal conifer stands," *Agricult. Forest Meteorol.*, vol. 80, nos. 2–4, pp. 135–163, Jul. 1996.

[10] Y. Ryu *et al.*, "On the correct estimation of effective leaf area index: Does it reveal information on clumping effects?" *Agricult. Forest Meteorol.*, vol. 150, no. 3, pp. 463–472, Mar. 2010.

[11] G. Yan *et al.*, "Review of indirect methods for leaf area index measurement," *J. Remote Sens.*, vol. 20, no. 5, pp. 958–978, 2016.

[12] F. Baret *et al.*, "GEOV1: *LAI* and *FAPAR* essential climate variables and *FCOVER* global time series capitalizing over existing products. Part1: Principles of development and production," *Remote Sens. Environ.*, vol. 137, pp. 299–309, Oct. 2013.

[13] S. Liang *et al.*, "A long-term Global LAnd Surface Satellite (GLASS) data-set for environmental studies," *Int. J. Digit. Earth*, vol. 6, pp. 5–33, Jul. 2013.

[14] R. B. Myneni *et al.*, "Global products of vegetation leaf area and fraction absorbed PAR from year one of MODIS data," *Remote Sens. Environ.*, vol. 83, nos. 1–2, pp. 214–231, Nov. 2002.

[15] P. L. Nagler, E. P. Glenn, T. L. Thompson, and A. Huete, "Leaf area index and normalized difference vegetation index as predictors of canopy characteristics and light interception by riparian species on the Lower Colorado River," *Agricult. Forest Meteorol.*, vol. 125, nos. 1–2, pp. 1–17, Sep. 2004.

[16] A. A. Abuelgasim, R. A. Fernandes, and S. G. Leblanc, "Evaluation of national and global LAI products derived from optical remote sensing instruments over Canada," *IEEE Trans. Geosci. Remote Sens.*, vol. 44, no. 7, pp. 1872–1884, Jul. 2006.

[17] K. Yan *et al.*, "Evaluation of MODIS LAI/FPAR product collection 6. Part 2: Validation and intercomparison," *Remote Sens.*, vol. 8, no. 6, p. 460, 2016.

[18] H. L. Fang, S. Wei, C. Jiang, and K. Scipal, "Theoretical uncertainty analysis of global MODIS, CYCLOPES, and GLOBCARBON LAI products using a triple collocation method," *Remote Sens. Environ.*, vol. 124, pp. 610–621, Sep. 2012.

[19] H. Ren, G. Yan, R. Liu, F. Nerry, Z.-L. Li, and R. Hu, "Impact of sensor footprint on measurement of directional brightness temperature of row crop canopies," *Remote Sens. Environ.*, vol. 134, pp. 135–151, Jul. 2013.

[20] M. Bouvier, S. Durrieu, R. A. Fournier, and J.-P. Renaud, "Generalizing predictive models of forest inventory attributes using an area-based approach with airborne LiDAR data," *Remote Sens. Environ.*, vol. 156, pp. 322–334, Jan. 2015.

[21] M. A. Lefsky, W. B. Cohen, G. G. Parker, and D. J. Harding, "Lidar remote sensing for ecosystem studies: Lidar, an emerging remote sensing technology that directly measures the three-dimensional distribution of plant canopies, can accurately estimate vegetation structural attributes and should be of particular interest to forest, landscape, and global ecologists," *Bioscience*, vol. 52, no. 1, pp. 19–30, Jan. 2002.

[22] D. Riaño, F. Valladares, S. Condés, and E. Chuvieco, "Estimation of leaf area index and covered ground from airborne laser scanner (Lidar) in two contrasting forests," *Agricult. Forest Meteorol.*, vol. 124, nos. 3–4, pp. 269–275, Aug. 2004.

[23] K. Lim, P. Treitz, M. Wulder, B. St-Onge, and M. Flood, "LiDAR remote sensing of forest structure," *Prog. Phys. Geogr., Earth Environ.*, vol. 27, no. 1, pp. 88–106, Mar. 2003.

[24] J. J. Richardson, L. M. Moskal, and S.-H. Kim, "Modeling approaches to estimate effective leaf area index from aerial discrete-return LIDAR," *Agricult. Forest Meteorol.*, vol. 149, nos. 6–7, pp. 1152–1160, Jun. 2009.

[25] F. Zhao *et al.*, "Measuring effective leaf area index, foliage profile, and stand height in New England forest stands using a full-waveform ground-based lidar," *Remote Sens. Environ.*, vol. 115, no. 11, pp. 2954–2964, Nov. 2011.

[26] H. Tang *et al.*, "Deriving and validating Leaf Area Index (LAI) at multiple spatial scales through lidar remote sensing: A case study in Sierra National Forest, CA," *Remote Sens. Environ.*, vol. 143, pp. 131–141, Mar. 2014.

[27] F. Morsdorf, B. Kötz, E. Meier, K. I. Itten, and B. Allgöwer, "Estimation of LAI and fractional cover from small footprint airborne laser scanning data based on gap fraction," *Remote Sens. Environ.*, vol. 104, no. 1, pp. 50–61, Sep. 2006.

[28] J. Heiskanen, L. Korhonen, J. Hietanen, and P. K. E. Pellikka, "Use of airborne lidar for estimating canopy gap fraction and leaf area index of tropical montane forests," *Int. J. Remote Sens.*, vol. 36, no. 10, pp. 2569–2583, 2015.

[29] S. Z. Luo *et al.*, "Estimation of wetland vegetation height and leaf area index using airborne laser scanning data," *Ecol. Indicators*, vol. 48, pp. 550–559, Jan. 2015.

[30] T. A. Black, J.-M. Chen, X. Lee, and R. M. Sagar, "Characteristics of shortwave and longwave irradiances under a Douglas-fir forest stand," *Can. J. Forest Res.*, vol. 21, no. 7, pp. 1020–1028, Jul. 1991.

[31] J. M. Chen and T. A. Black, "Measuring leaf area index of plant canopies with branch architecture," *Agricult. Forest Meteorol.*, vol. 57, nos. 1–3, pp. 1–12, Dec. 1991.

[32] J. L. Lovell, D. L. B. Jupp, D. S. Culvenor, and N. C. Coops, "Using airborne and ground-based ranging lidar to measure canopy structure in Australian forests," *Can. J. Remote Sens.*, vol. 29, no. 5, pp. 607–622, Oct. 2003.

[33] C. Hopkinson, J. Lovell, L. Chasmer, D. Jupp, N. Kljun, and E. van Gorsel, "Integrating terrestrial and airborne lidar to calibrate a 3D canopy model of effective leaf area index," *Remote Sens. Environ.*, vol. 136, pp. 301–314, Sep. 2013.

[34] F. D. Schneider *et al.*, "Simulating imaging spectrometer data: 3D forest modeling based on LiDAR and *in situ* data," *Remote Sens. Environ.*, vol. 152, pp. 235–250, Sep. 2014.

[35] G. Zheng and L. M. Moskal, "Retrieving leaf area index (LAI) using remote sensing: Theories, methods and sensors," *Sensors*, vol. 9, no. 4, pp. 2719–2745, Apr. 2009.

[36] F. Hosoi and K. Omasa, "Factors contributing to accuracy in the estimation of the woody canopy leaf area density profile using 3D portable lidar imaging," *J. Experim. Botany*, vol. 58, no. 12, pp. 3463–3473, Oct. 2007.

[37] H. Tang *et al.*, "Retrieval of vertical LAI profiles over tropical rain forests using waveform lidar at La Selva, Costa Rica," *Remote Sens. Environ.*, vol. 124, pp. 242–250, Sep. 2012.

[38] K. Zhao and S. Popescu, "Lidar-based mapping of leaf area index and its use for validating GLOBCARBON satellite LAI product in a temperate forest of the southern USA," *Remote Sens. Environ.*, vol. 113, no. 8, pp. 1628–1645, Aug. 2009.

[39] J. L. R. Jensen, K. S. Humes, L. A. Vierling, and A. T. Hudak, "Discrete return lidar-based prediction of leaf area index in two conifer forests," *Remote Sens. Environ.*, vol. 112, no. 10, pp. 3947–3957, Oct. 2008.

[40] J. Zou, G. Yan, and L. Chen, "Estimation of canopy and woody components clumping indices at three mature picea crassifolia forest stands," *IEEE Trans. Geosci. Remote Sens.*, vol. 8, no. 4, pp. 1413–1422, Apr. 2015.

[41] J. Pisek *et al.*, "Retrieving vegetation clumping index from Multi-angle Imaging SpectroRadiometer (MISR) data at 275 m resolution," *Remote Sens. Environ.*, vol. 138, pp. 126–133, Nov. 2013.

[42] V. Thomas, T. Noland, P. Treitz, and J. H. McCaughey, "Leaf area and clumping indices for a boreal mixed-wood forest: Lidar, hyperspectral, and Landsat models," *Int. J. Remote Sens.*, vol. 32, no. 23, pp. 8271–8297, 2011.

[43] M. García, J. Gajardo, D. Riaño, K. Zhao, P. Martín, and S. Ustin, "Canopy clumping appraisal using terrestrial and airborne laser scanning," *Remote Sens. Environ.*, vol. 161, pp. 78–88, May 2015.

[44] Y. Zeng *et al.*, "Extracting leaf area index by sunlit foliage component from downward-looking digital photography under clear-sky conditions," *Remote Sens.*, vol. 7, no. 10, pp. 13410–13435, 2015.

[45] R. Hu, J. Luo, G. Yan, J. Zou, and X. Mu, "Indirect measurement of forest leaf area index using path length distribution model and multispectral canopy imager," *IEEE Trans. Geosci. Remote Sens.*, vol. 9, no. 6, pp. 2532–2539, Jun. 2016.

[46] W. Woodgate *et al.*, "An improved theoretical model of canopy gap probability for Leaf Area Index estimation in woody ecosystems," *Forest Ecol. Manage.*, vol. 358, pp. 303–320, Dec. 2015.

[47] M. Alonzo, B. Bookhagen, J. P. McFadden, A. Sun, and D. A. Roberts, "Mapping urban forest leaf area index with airborne lidar using penetration metrics and allometry," *Remote Sens. Environ.*, vol. 162, pp. 141–153, Jun. 2015.

[48] L. Korhonen, I. Korpela, J. Heiskanen, and M. Maltamo, "Airborne discrete-return LIDAR data in the estimation of vertical canopy cover, angular canopy closure and leaf area index," *Remote Sens. Environ.*, vol. 115, no. 4, pp. 1065–1080, Apr. 2011.

[49] X. Tian *et al.*, "The complicate observations and multi-parameter land information constructions on allied telemetry experiment (COMPLICATE)," *PLoS ONE*, vol. 10, no. 9, p. e0137545, Sep. 2015.

[50] C. Macfarlane, A. Grigg, and C. Evangelista, "Estimating forest leaf area using cover and fullframe fisheye photography: Thinking inside the circle," *Agricult. Forest Meteorol.*, vol. 146, nos. 1–2, pp. 1–12, Sep. 2007.

[51] X. Mu *et al.*, "Evaluation of sampling methods for validation of remotely sensed fractional vegetation cover," *Remote Sens.*, vol. 7, no. 12, pp. 16164–16182, Dec. 2015.

[52] C. Macfarlane, Y. Ryu, G. N. Ogden, and O. Sonnentag, "Digital canopy photography: Exposed and in the raw," *Agricult. Forest Meteorol.*, vol. 197, pp. 244–253, Oct. 2014.

[53] Y. Hwang *et al.*, "Correction for light scattering combined with sub-pixel classification improves estimation of gap fraction from digital cover photography," *Agricult. Forest Meteorol.*, vol. 222, pp. 32–44, May 2016.

[54] Y. Ryu *et al.*, "Continuous observation of tree leaf area index at ecosystem scale using upward-pointing digital cameras," *Remote Sens. Environ.*, vol. 126, pp. 116–125, Nov. 2012.

[55] J. Pisek, O. Sonnentag, A. D. Richardson, and M. Mõttus, "Is the spherical leaf inclination angle distribution a valid assumption for temperate and boreal broadleaf tree species?" *Agricult. Forest Meteorol.*, vol. 169, pp. 186–194, Feb. 2013.
[56] M. Isenburg. *LAStools—Efficient LiDAR Processing Software*. Accessed: Sep. 17, 2017.[Online]. Available: http://rapidlasso.com/LAStools
[57] P. E. Axelsson, "DEM generation from laser scanner data using adaptive TIN models," in *Proc. Int. Archiv. Photogram. Remote Sens.*, vol. 33. Amsterdam, The Netherlands, 2000, pp. 110–117.
[58] J. Ross, *The Radiation Regime and Architecture of Plant Stands*, vol. 3. The Hague, The Netherlands: Dr. W. Junk Publishers, 1981.
[59] S. B. Jennings, N. D. Brown, and D. Sheil, "Assessing forest canopies and understorey illumination: Canopy closure, canopy cover and other measures," *Forestry*, vol. 72, no. 1, pp. 59–73, 1999.
[60] S. Solberg *et al.*, "Mapping LAI in a Norway spruce forest using airborne laser scanning," *Remote Sens. Environ.*, vol. 113, no. 11, pp. 2317–2327, Nov. 2009.
[61] A. Khosravipour *et al.*, "Generating pit-free canopy height models from airborne lidar," *Photogram. Eng. Remote Sens.*, vol. 80, no. 9, pp. 863–872, Sep. 2014.
[62] W. M. Zhang *et al.*, "An easy-to-use airborne LiDAR data filtering method based on cloth simulation," *Remote Sens.*, vol. 8, no. 6, p. 501, Jun. 2016.

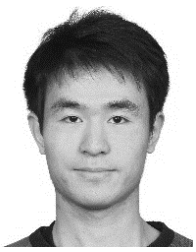

Ronghai Hu is currently pursuing the Ph.D. degree with Beijing Normal University, Beijing, China. He is also a joint Student with the ICube Laboratory, CNRS-University of Strasbourg, Illkirch, France.

His research interests include the indirect leaf area index measurement, vegetation remote sensing, LiDAR, and scale effect on remote sensing.

Guangjian Yan (SM'16) received the Ph.D. degree from the Institute of Remote Sensing Applications, Chinese Academy of Sciences, Beijing, China, in 1999.

He is currently a Professor with the State Key Laboratory of Remote Sensing Science, School of Geography, Beijing Normal University, Beijing. He has authored more than 200 papers. His research interests include multiangular remote sensing, vegetation remote sensing, scale effect, and scale correction of remote sensing.

Françoise Nerry received the Ph.D. degree from the University of Strasbourg, Strasbourg, France, in 1988.

Since 1990, she has been a Permanent Researcher with the Image Sciences, Computer Sciences and Remote Sensing Laboratory (LSIIT), CNRS, Illkirch, France, which changed to ICube in 2013. She is also the Head of the TRIO/ICube Team involving 40 persons, including 20 permanents. She has been involved in numerous national and international programs. Her research interests include thermal infrared radiometry and methodology of physical analysis of remote sensing data.

Yunshu Liu received the B.S. degree in geographic information science from the School of Geography, Beijing Normal University, Beijing, China. He is currently pursuing the master's degree from Peking University, Beijing.

His research interests include vegetation remote sensing and geographic information system.

Yumeng Jiang received the B.Sc. degree from Beijing Normal University, Beijing, China.

Her research interests include geographic information system and vegetation remote sensing.

Shuren Wang received a B.Sc. degree from Beijing Normal University, Beijing, China, where she is currently pursuing the master's degree.

Her research interests include laser penetration index measurement and vegetation remote sensing.

Yiming Chen is currently pursuing the Ph.D. degree in cartography and geographic information system from the School of Geography, Beijing Normal University, Beijing, China. He is also a joint Student with Boston University, Boston, MA, USA.

His research interests include using remote sensing to retrieve canopy structural parameters, processing LiDAR point cloud, and building modeling.

Xihan Mu received the B.S. degree in computer science and technology from the College of Information Science and Technology, Beijing Normal University, Beijing, China, in 1999, and the Ph.D. degree in remote sensing from the School of Geography, Beijing Normal University, in 2009.

He was a Visiting Student with the Laboratoire des Sciences de l'Images, de l'Informatique et de la Télédétection, Louis Pasteur University, Strasbourg, France, in 2007, and also with the Commonwealth Scientific and Industrial Research Organisation, Canberra, ACT, Australia, in 2016. He is currently with the State Key Laboratory of Remote Sensing Science, School of Geography, Beijing Normal University. His research interests include using multiangular remote sensing to retrieve vegetation structural parameters and land-surface temperature.

Wuming Zhang received the Ph.D. degree in material science and engineering from Tsinghua University, Beijing, China.

He is currently with the State Key Laboratory of Remote Sensing Science, School of Geography, Beijing Normal University, Beijing. His research interests include 3-D digitization, multisensor data fusion, and remote sensing data processing and inversion.

Donghui Xie received the Ph.D. degree in remote sensing and geographic information systems from Beijing Normal University, Beijing, China, in 2005.

From 2005 to 2007, she was a Post-Doctoral Research Associate with Beijing Normal University, where she is currently with the State Key Laboratory of Remote Sensing Science, Institute of Remote Sensing Science and Engineering, Faculty of Geographical Science. Her research interests include canopy radiative transfer modeling and biophysical parameter retrieval of vegetation.